nature chemical biology

Supplementary information

https://doi.org/10.1038/s41589-025-01836-0

Quinone extraction drives atmospheric carbon monoxide oxidation in bacteria

In the format provided by the authors and unedited

Supplementary Information

Table of Contents

Supplementary Figures

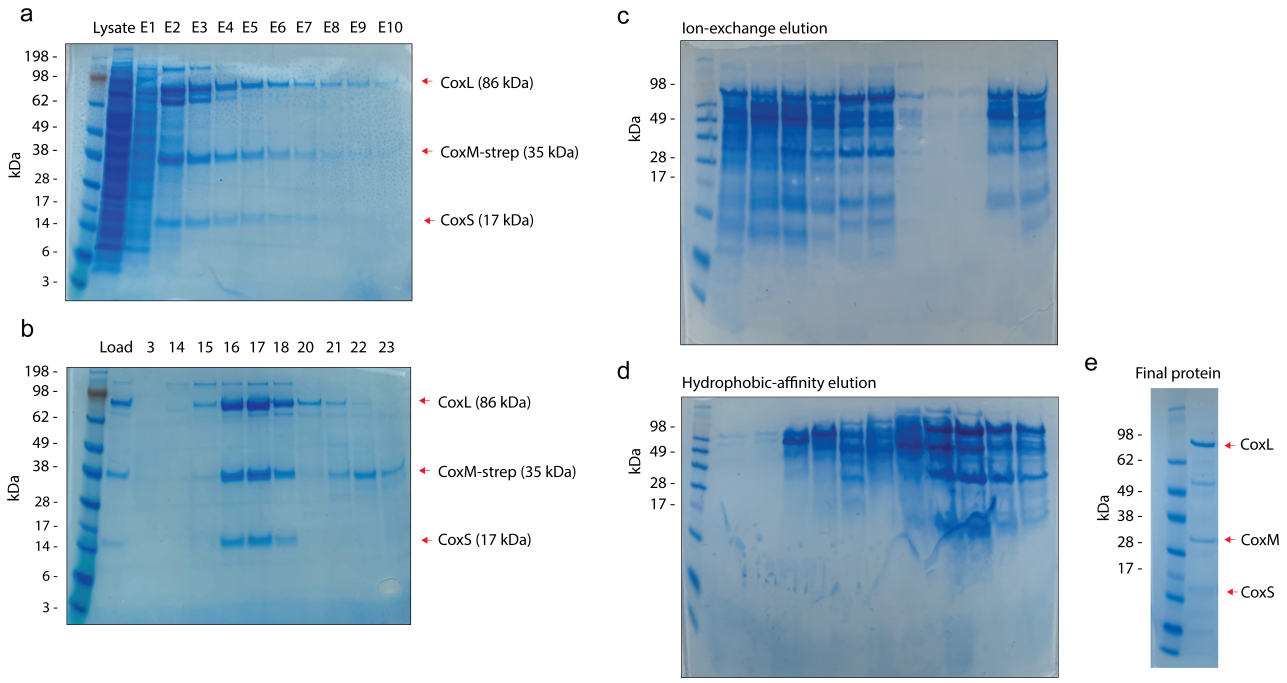

Supplementary Figure 1. Native purification of Mo-CODH$_{Ms}$ and Mo-CODH$_{Ac}$. (a) SDS-PAGE of Mo-CODH$_{Ms}$ after strep-trap isolation. Labels refer to elution fraction. **(b)** SDS-PAGE of Mo-CODH$_{Ms}$ after SEC, demonstrating the final purity of the sample. Labels refer to elution fraction. **(c)** SDS-PAGE of Mo-CODH$_{Ac}$ after ion-exchange chromatography. **(d)** SDS-PAGE of Mo-CODH$_{Ac}$ after hydrophobic affinity chromatography. **(e)** Final purified Mo-CODH$_{Ac}$ used for activity measurements.

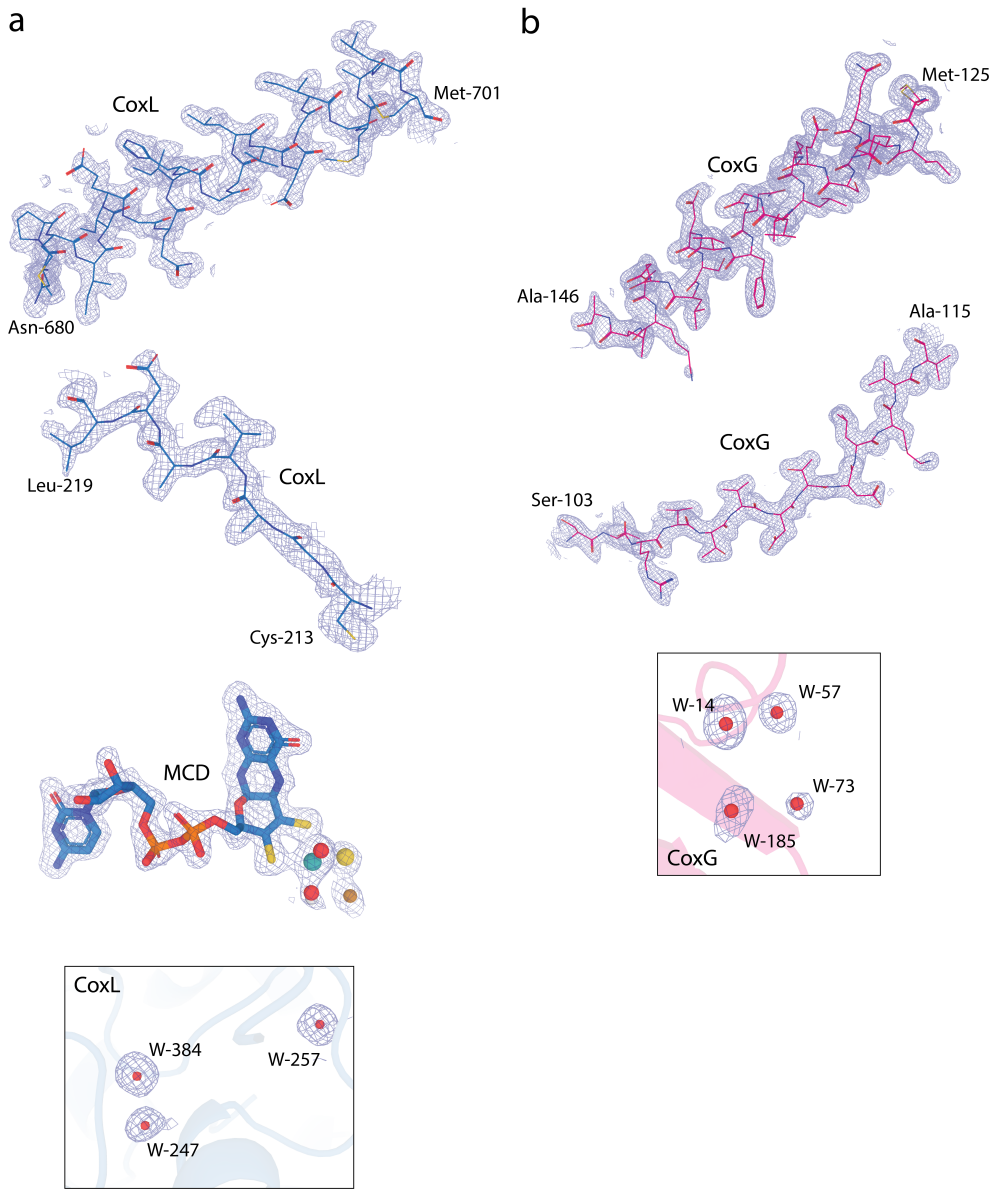

Supplementary Figure 2. Representative density maps from the Mo-CODH$_{Ms}$ and CoxG$_{NT}$ structures. (a) Representative Coulomb potential density from the Mo-CODH Cryo-EM maps contoured at 4 σ. (b) Representative electron density from the CoxG$_{NT}$ 2Fo-Fc maps contoured at 1 σ.

Supplementary Tables

Supplementary Table 1. Mo-CODH$_{Ms}$ cryoEM data collection and model refinement statistics All datasets were collected with a zero-loss filtering slit width of 10 eV and with 60 frames per movie.

	CODH (EMD-42164) (PDB 8UEM)
Data collection and processing	
Magnification	105kx
Voltage (kV)	300
Electron exposure (e–/Å^2)	66.0
Defocus range (μm)	-1.5-0.5
Pixel size (Å)	0.82
Symmetry imposed	C2
Initial particle images (no.)	1,034,005
Final particle images (no.)	290,597
Map resolution (Å)	1.85
FSC threshold	0.143
Map resolution range (Å)	1.85 – 2.44
Refinement	
Initial model used (PDB code)	-
Model resolution (Å)	1.85
FSC threshold	0.143
Model resolution range (Å)	n/a
Map sharpening *B* factor (Å^2)	38.1
Map-Model CC	0.85
Model composition	
Non-hydrogen atoms	19599
Protein residues	2450
Ligands	10
Solvent	899
B factors (Å^2)	
Protein	19.98
Ligand	11.52
Solvent	22.82
R.m.s. deviations	
Bond lengths (Å)	0.010
Bond angles (°)	1.179
Validation	
MolProbity score	1.57
Clashscore	8.24
Poor rotamers (%)	0.52
Ramachandran plot	
Favored (%)	97.37
Allowed (%)	2.55
Disallowed (%)	0.08

Supplementary Table 2. $CoxG_{NT}$ X-ray crystallography data collection and model refinement statistics

	CoxG
Data Collection[a]	
Space Group	*P 4₃ 2₁ 2*
Cell Dimensions	
a, b, c (Å)	64.09 64.09 87.54
α, β, γ (°)	90 90 90
Wavelength	0.976
Resolution (Å)	45.33-1.50 (1.52-1.50)
R_{merge}	0.63 (4.206)
R_{pim}	0.013 (1.032)
I/s(*I*)	32.9 (1.2)
CC(1/2)	1.00 (0.624)
Completeness (%)	100.0 (100.0)
Redundancy	42.4 (33.7)
No. reflection	29999 (1463)
Refinement statistics	
R_{work}/R_{free}	18.10/22.72
No. atoms	
Protein	1145
Ligand / ions	0
Solvent	176
R.m.s deviations	
Bond lengths (Å)	0.006
Bond angles (°)	0.87
Ramachandran Plot	
Favored/Allowed/Outliers (%)	98.62/1.38/0.00
Clash Score	6.49
Average B-factor	37.26
PDB ID	8UDS

[a] Values in parentheses are for highest-resolution shell.
Data from one crystal was collected for each structure

Supplementary Table 3. AlphaFold2 model CoxG-Mo-CODH interface statistics

	M. smegmatis CODH	*M. smegmatis* XOF	*B. japonicum* CODH	*T. carboxidovorans* CODH	*A. carboxidovorans* CODH	*C. thermoautotrophica* CODH	*A. ehrlichii* CODH	*N. tibetense* CODH
Interface Area (Å)	1328	1325	2118	1274	1198	1281	2022	1424
Delta G (kCal/mol)	-7.9	-7.1	-13.3	-9.5	-11.2	-6.5	-12.9	-1.3
Binding Energy (kCal/mol)	-12.9	-11.3	-25.3	-14.4	-15.6	-12.7	-21.7	-14.8
P-value	0.3449	0.3906	0.2713	0.3169	0.3417	0.4525	0.226	0.4107
Hydrogen Bonds	7	7	12	5	4	9	13	12
Salt Bridges	5	3	18	7	7	6	8	22
Disulphide bonds	0	0	0	0	0	0	0	0

Supplementary Table 4. AlphaFold2 model CoxG-Mo-CODH salt bridge interactions

Bond Distance (Å)	Mo-CODH	CoxG
	***M. Smegmatis* CODH**	
3	A:GLU 927 [OE2]	D:LYS 50 [NZ] res:[825 : 49]
2.6	A:ASP 139 [OD1]	D:LYS 81 [NZ] res:[138 : 80]
2.7	A:ASP 709 [OD1]	D:LYS 113 [NZ] res:[708 : 112]
2.6	A:GLU1060 [OE2]	D:LYS 132 [NZ] res:[958 : 131]
3.5	**A:GLU1060 [OE1]**	**D:LYS 132 [NZ] res:[958 : 131]**
	***M. smegmatis* XOF**	
3.2	A:ASP 926 [OD2]	D:LYS 50 [NZ] res:[809 : 49]
3.1	A:ASP 690 [OD1]	D:ARG 124 [NE] res:[689 : 123]
2.7	A:ASP 690 [OD1]	D:ARG 124 [NH2] res:[689 : 123]
	***T. carboxidovorans* CODH**	
3.8	A:ASP1127 [OD1]	D:LYS 56 [NZ] res:[987 : 55]
2.7	A:ASP 131 [OD1]	D:LYS 81 [NZ] res:[130 : 80]
3.1	A:ASP1220 [OD2]	D:ARG 123 [NH1] res:[1080 : 122]
2.7	A:ASP1220 [OD1]	D:ARG 123 [NH1] res:[1080 : 122]
2.7	A:ASP1220 [OD2]	D:ARG 123 [NH2] res:[1080 : 122]
3.7	A:ASP1220 [OD1]	D:ARG 123 [NH2] res:[1080 : 122]
2.6	A:GLU1259 [OE2]	D:LYS 131 [NZ] res:[1119 : 130]
	***N. tibetense* CODH**	
3.5	A:ARG 79 [NH1]	D:GLU 93 [OE1] res:[78 : 92]
2.7	A:ARG 79 [NH2]	D:GLU 93 [OE1] res:[78 : 92]
2.7	A:ARG 79 [NH1]	D:GLU 93 [OE2] res:[78 : 92]
3.4	A:ARG 79 [NH2]	D:GLU 93 [OE2] res:[78 : 92]
2.9	A:GLU1262 [OE1]	D:LYS 32 [NZ] res:[1148 : 31]
3.8	A:ASP1126 [OD2]	D:ARG 91 [NE] res:[1012 : 90]
3.5	A:GLU1148 [OE1]	D:ARG 91 [NH1] res:[1034 : 90]
2.9	A:GLU1148 [OE1]	D:ARG 91 [NH2] res:[1034 : 90]
2.6	A:ASP1126 [OD2]	D:ARG 91 [NH2] res:[1012 : 90]
2.7	A:ASP 724 [OD2]	D:ARG 151 [NH1] res:[723 : 150]
2.7	A:ASP 724 [OD2]	D:ARG 151 [NH2] res:[723 : 150]
3.4	A:ASP1359 [OD2]	D:ARG 158 [NE] res:[1245 : 157]
3.3	A:ASP1359 [OD2]	D:ARG 158 [NH1] res:[1245 : 157]
2.7	A:ASP1359 [OD1]	D:ARG 158 [NH1] res:[1245 : 157]
3.8	A:ASP1359 [OD2]	D:ARG 158 [NH2] res:[1245 : 157]
2.6	A:ASP1257 [OD2]	D:LYS 166 [NZ] res:[1143 : 165]
	***C. thermoautotrophica* CODH**	
3.8	A:ARG 792 [NH2]	D:ASP 110 [OD2] res:[791 : 109]
2.9	A:GLU 697 [OE1]	D:MET 1 [N] res:[696 : 0]
3.2	A:ASP1221 [OD2]	D:ARG 123 [NH1] res:[1075 : 122]
2.7	A:ASP1221 [OD1]	D:ARG 123 [NH1] res:[1075 : 122]
2.7	A:ASP1221 [OD2]	D:ARG 123 [NH2] res:[1075 : 122]

3.6	A:ASP1221 [OD1]	D:ARG 123 [NH2] res:[1075 : 122]
	***B. japonicum* CODH**	
3.8	A:ARG1344 [NH1]	D:ASP 955 [OD2] res:[1242 : 127]
3.4	A:ARG1344 [NE]	D:ASP 955 [OD2] res:[1242 : 127]
2.8	A:ARG1344 [NH1]	D:ASP 955 [OD1] res:[1242 : 127]
3.8	A:ARG1344 [NE]	D:ASP 955 [OD1] res:[1242 : 127]
3.4	A:ASP 827 [OD1]	D:ARG 828 [N] res:[826 : 0]
3.2	A:ASP 827 [OD2]	D:ARG 829 [NE] res:[826 : 1]
2.8	A:ASP 827 [OD1]	D:ARG 829 [NE] res:[826 : 1]
2.7	A:ASP 827 [OD2]	D:ARG 829 [NH2] res:[826 : 1]
3.8	A:ASP 827 [OD1]	D:ARG 829 [NH2] res:[826 : 1]
2.7	A:ASP 827 [OD2]	D:ARG 831 [NH2] res:[826 : 3]
3.6	A:GLU 138 [OE1]	D:ARG 889 [NH1] res:[137 : 61]
3.4	A:ASP1220 [OD2]	D:ARG 952 [NH1] res:[1118 : 124]
2.7	A:ASP1220 [OD1]	D:ARG 952 [NH1] res:[1118 : 124]
2.7	A:ASP1220 [OD2]	D:ARG 952 [NH2] res:[1118 : 124]
3.5	A:ASP1220 [OD1]	D:ARG 952 [NH2] res:[1118 : 124]
2.8	A:ASP1315 [OD2]	D:ARG 959 [NE] res:[1213 : 131]
2.6	A:ASP1315 [OD2]	D:ARG 959 [NH2] res:[1213 : 131]
4	A:ASP1315 [OD1]	D:ARG 959 [NH2] res:[1213 : 131]
	***A. carboxidovorans* CODH**	
3.9	A:GLU1126 [OE2]	D:ARG 51 [NE] res:[1000 : 50]
3.7	A:ASP1127 [OD2]	D:ARG 51 [NH2] res:[1001 : 50]
3	A:ASP1127 [OD2]	D:LYS 56 [NZ] res:[1001 : 55]
3.4	A:ASP1220 [OD1]	D:ARG 123 [NH1] res:[1094 : 122]
2.9	A:ASP1220 [OD2]	D:ARG 123 [NH1] res:[1094 : 122]
2.7	A:ASP1220 [OD1]	D:ARG 123 [NH2] res:[1094 : 122]
3.6	A:ASP1220 [OD2]	D:ARG 123 [NH2] res:[1094 : 122]
	***A. ehrlichii* CODH**	
2.7	C:GLU1155 [OE1]	D:LYS 817 [NZ] res:[1068 : 2]
2.6	C:GLU1155 [OE2]	D:LYS 817 [NZ] res:[1068 : 2]
2.7	C:GLU 926 [OE2]	D:LYS 890 [NZ] res:[839 : 75]
2.6	C:GLU 947 [OE1]	D:LYS 924 [NZ] res:[860 : 109]
3	C:GLU 947 [OE2]	D:LYS 924 [NZ] res:[860 : 109]
3.8	C:ASP1020 [OD1]	D:ARG 965 [NE] res:[933 : 150]
2.8	C:ASP1020 [OD1]	D:ARG 965 [NH2] res:[933 : 150]
2.7	C:ASP1020 [OD2]	D:ARG 965 [NH2] res:[933 : 150]

Supplementary Table 5. Occurrence of *coxG* in the Mo-CODH gene cluster in diverse bacteria and archaea

Genebank ID	Species	*coxG* Present in Cox Gene cluster
>WP_003892166.1	*Mycolicibacterium smegmatis*	Yes
>WP_003900133.1	*Mycobacterium tuberculosis*	Yes
>WP_005512167.1	*Rhodococcus hoagie*	Yes
>WP_006337626.1	*Gordonia rhizosphera*	No (Xath. Ox Present which does)
>WP_052603923.1	*Acidithrix ferrooxidans*	No (Xath. Ox Present which does)
>WP_100668643.1	*Kyrpidia spormannii*	Yes
>WP_035348617.1	*Edaphobacter aggregans*	Yes
>WP_052889641.1	*Thermogemmatispora carboxidivorans*	Yes
>WP_006092369.1	*Natronorubrum tibetense*	Yes
>WP_004434061.1	*Bacillus methanolicus*	Yes
>WP_007909428.1	*Ktedonobacter racemifer*	Yes
>WP_004436402.1	*Bacillus methanolicus*	Yes
>WP_207270240.1	*Haloterrigena longa*	Yes
>WP_008163357.1	*Natronorubrum sulfidifaciens*	Yes
>WP_049982621.1	*Halorubrum sp. BV1*	Yes
>WP_144901421.1	*Halobellus captivus*	Yes
>WP_012642423.1	*Thermomicrobium roseum*	No (Xath. Ox Present which does)
>WP_079512197.1	*Maribacter arcticus*	Yes
>WP_011629305.1	*Alkalilimnicola ehrlichii*	Yes (Fusion with CoxL)
>MBP1960087.1	*Aminobacter sp.*	No (Homologues in genome)
>WP_012715912.1	*Sulfolobus islandicus*	No
>WP_006934453.1	*Roseibium aggregatum*	Yes
>WP_048100679.1	*Candidatus Acidianus copahuensis*	No
>WP_067068110.1	*Streptomyces thermoautotrophicus*	Yes
>WP_038955575.1	*Bradyrhizobium japonicum*	Yes (Fusion with CoxL)
>WP_013913730.1	*Oligotropha carboxidovorans*	Yes
>WP_043833835.1	*Amycolatopsis orientalis*	Yes
>WP_171911943.1	*Paraburkholderia xenovorans*	Yes
>WP_011048110.1	*Ruegeria pomeroyi*	Yes
>QBR71171.1	*Methylocapsa gorgona*	Yes

Supplementary Table 6. Mo-CODH subunit sequence identity percentage matrices

CoxG		WP_039150234.1	WP_066886512.1	WP_013913734.1	WP_052889639.1	ABI56911.1	A0A4P6WWM5	ABK73218.1	WP_011730864.1	WP_006092373.1
		***B. japonicum* CODH**	***C. thermoautotrophica* CODH**	***A. carboxidovorans* CODH**	***T. carboxidivorans* CODH**	***A. ehrlichii* CODH**	***H. pseudoflava* CODH**	***M. smegmatis* CODH**	***M. smegmatis* XOF**	***N. tibetense* CODH**
WP_039150234.1	***B. japonicum* CODH**	100	38	38	27	24	21	20	20	23
WP_066886512.1	***C. thermoautotrophica* CODH**	38	100	37	29	17	21	28	24	21
WP_013913734.1	***A. carboxidovorans* CODH**	38	37	100	33	21	26	25	25	26
WP_052889639.1	***T. carboxidivorans* CODH**	27	29	33	100	20	25	28	25	28
ABI56911.1	***A. ehrlichii* CODH**	24	17	21	20	100	41	31	26	18
A0A4P6WWM5	***H. pseudoflava* CODH**	21	21	26	25	41	100	35	27	22
ABK73218.1	***M. smegmatis* CODH**	20	28	25	28	31	35	100	53	23
WP_011730864.1	***M. smegmatis* XOF**	20	24	25	25	26	27	53	100	23
WP_006092373.1	***N. tibetense* CODH**	23	21	26	28	18	22	23	23	100

CoxL		ABI56911.1	A0A4P6WU61	WP_013913730.1	WP_052889641.1	YP_885152.1	WP_006092369.1	WP_232778399.1	WP_011730863.1	WP_039150234.1
		***A. ehrlichii* CODH**	***H. pseudoflava* CODH**	***A. carboxidovorans* CODH**	***T. carboxidivorans* CODH**	***M. smegmatis* CODH**	***N. tibetense* CODH**	***C. thermoautotrophica* CODH**	***M. smegmatis* XOF**	***B. japonicum* CODH**
ABI56911.1	***A. ehrlichii* CODH**	100	73	70	61	57	59	53	33	31
A0A4P6WU61	***H. pseudoflava* CODH**	73	100	67	62	59	59	54	33	30
WP_013913730.1	***A. carboxidovorans* CODH**	70	67	100	61	56	55	54	33	30
WP_052889641.1	***T. carboxidivorans* CODH**	61	62	61	100	63	61	58	36	34
YP_885152.1	***M. smegmatis* CODH**	57	59	56	63	100	61	56	37	34
WP_006092369.1	***N. tibetense* CODH**	59	59	55	61	61	100	54	35	30
WP_232778399.1	***C. thermoautotrophica* CODH**	53	54	54	58	56	54	100	33	31
WP_011730863.1	***M. smegmatis* XOF**	33	33	33	36	37	35	33	100	31
WP_039150234.1	***B. japonicum* CODH**	31	30	30	34	34	30	31	31	100

CoxM		ABI56909.1	A0A4P6WSZ1	WP_013913728.1	YP_885150.1	WP_067068118.1	WP_006092371.1	WP_052889643.1	WP_039150231.1	WP_011730865.1
		***A. ehrlichii* CODH**	***H. pseudoflava* CODH**	***A. carboxidovorans* CODH**	***M. smegmatis* CODH**	***C. thermoautotrophica* CODH**	***N. tibetense* CODH**	***T. carboxidivorans* CODH**	***B. japonicum* CODH**	***M. smegmatis* XOF**
ABI56909.1	***A. ehrlichii* CODH**	100	57	50	41	41	39	47	31	35
A0A4P6WSZ1	***H. pseudoflava* CODH**	57	100	53	40	43	41	48	34	37
WP_013913728.1	***A. carboxidovorans* CODH**	50	53	100	39	36	35	44	31	36
YP_885150.1	***M. smegmatis* CODH**	41	40	39	100	39	37	42	29	33
WP_067068118.1	***C. thermoautotrophica* CODH**	41	43	36	39	100	47	50	33	38
WP_006092371.1	***N. tibetense* CODH**	39	41	35	37	47	100	46	30	36
WP_052889643.1	***T. carboxidivorans* CODH**	47	48	44	42	50	46	100	31	39
WP_039150231.1	***B. japonicum* CODH**	31	34	31	29	33	30	31	100	39
WP_011730865.1	***M. smegmatis* XOF**	35	37	36	33	38	36	39	39	100

CoxS		ABI56910.1	P19915	WP_013913729.1	WP_006092370.1	WP_052889642.1	WP_067068115.1	YP_885151.1	WP_011730866.1	WP_039150228.1
		***A. ehrlichii* CODH**	***H. pseudoflava* CODH**	***A. carboxidovorans* CODH**	***N. tibetense* CODH**	***T. carboxidivorans* CODH**	***C. thermoautotrophica* CODH**	***M. smegmatis* CODH**	***M. smegmatis* XOF**	***B. japonicum* CODH**
ABI56910.1	***A. ehrlichii* CODH**	100	74	62	55	59	60	53	45	42
P19915	***H. pseudoflava* CODH**	74	100	66	58	62	62	55	48	46
WP_013913729.1	***A. carboxidovorans* CODH**	62	66	100	60	59	56	53	48	43
WP_006092370.1	***N. tibetense* CODH**	55	58	60	100	66	61	59	49	46
WP_052889642.1	***T. carboxidivorans* CODH**	59	62	59	66	100	64	59	46	48
WP_067068115.1	***C. thermoautotrophica* CODH**	60	62	56	61	64	100	61	55	47
YP_885151.1	***M. smegmatis* CODH**	53	55	53	59	59	61	100	50	45
WP_011730866.1	***M. smegmatis* XOF**	45	48	48	49	46	55	50	100	48
WP_039150228.1	***B. japonicum* CODH**	42	46	43	46	48	47	45	48	100

Supplementary Table 7. Strains and plasmids used in this study

Primer Name	Sequence 5'-3'	Purpose
pX33 sequencing Fw	AATAGATCATCGTCGCCG	Screening of strep tag
pX33 seqeuncing Rv	TAATACGACTCACTATAGGG	Screening of strep tag
CoxG KO Fw	GCGAACGAGTTCACTGTGAGCGTG	Screening of coxG deletion
CoxG KO Rv	TCGATGCGGTGTTCTCCGACGC	Screening of coxG deletion
CoxG WT FL Fw	GTCAG GGATCCATGAAGATCGCGAACGAGTTCACTG	Amplification of coxG for complementation vector
CoxG WT FL Rv	GTCAGGAATTCTCATCTGCCGCGAAGGGCC	Amplification of coxG for complementation vector

Strain or plasmid	Relevant genotype and description	Reference or source
Escherichia coli K12 (DH5α)	Standard laboratory *E. coli* strain for plasmid propagation and maintenance	
Escherichia coli K12 (C41)	Standard laboratory *E. coli* strain for recombinant protein expression	
Mycobacterium smegmatis mc^2155	WT strain	Cordero et al. 2019 **[4]**
Mycobacterium smegmatis mc^2155 CoxM 2xStrepII	Isogenic strain to WT except with 2xStrep tag on CoxM C terminus	This study
Mycobacterium smegmatis mc^2155 CoxM 2xStrepII *ΔCoxG*	Isogenic strain to WT except with 2xStrep tag on CoxM C terminus and CoxG deletion	This study
pCoxM-2xStrepII	Allelic exchange vector for tagging CoxM with 2xStrep affinity tag. Geneblock containing CoxM2xStrepII ligated at SpeI sites into pX33 vector.	This study
p*ΔCoxG*	Allelic exchange vector for deletion of CoxG subunit. Geneblock containing CoxG flanks ligated at SpeI sites in pX33 vector.	This study
pCoxGtrunc	*E. coli* expression vector for CoxG recombinant expression. Truncated CoxG (missing the linker and membrane anchor) ligated into pET29b vector	This study
pCoxGWT	*M. smegmatis* complementation vector for CoxG. WT full length CoxG ligated into pMV261 at BamHI and EcoRI sites.	This study
pCoxG-KtoS	*M. smegmatis* complementation vector for CoxG. Mutated full length CoxG ligated into	This study

	pMV261 at BamHI and EcoRI sites. Select lysine residues at the predicted CoxG:MoCu-CODHMS interaction interface are mutated to serine residues.	
pCoxG-KtoD	*M. smegmatis* complementation vector for CoxG. Mutated full length CoxG ligated into pMV261 at BamHI and EcoRI sites. Select lysine residues at the predicted CoxG:MoCu-CODHMS interaction interface are mutated to aspartate residues.	This study
pCoxG-KtoE	*M. smegmatis* complementation vector for CoxG. Mutated full length CoxG ligated into pMV261 at BamHI and EcoRI sites. Select lysine residues at the predicted CoxG:MoCu-$CODH_{MS}$ interaction interface are mutated to glutamate residues.	This study

Supplementary Notes

Supplementary Note 1. Atmospheric CO oxidation by Mo-CODH$_{Ac}$

To assess the ability of other Mo-CODHs to oxidise atmospheric CO, we also analysed the activity of Mo-CODH$_{Ac}$, at low CO concentrations, both in cells and as purified enzyme. Firstly, we compared the activity of *M. smegmatis* and *A. carboxidovorans* cultures, at a starting headspace concentration of ~10 ppm CO. The bacteria consumed CO at a comparable rate, to near atmospheric concentrations (Extended Data Figure 1a). For this experiment, *A. carboxidovorans* was precultured under autotrophic conditions with a 50% CO headspace to maximise Mo-CODH expression. In contrast, *M. smegmatis* stationary phase cultures were utilised, as Mo-CODH is not induced by CO and the enzyme is maximally expressed during starvation [1]. These conditions were the same as we used for isolating Mo-CODH from these bacteria. Our purification yields for Mo-CODH were ~2 – 5 µg per litre of culture for *M. smegmatis* vs 1.2 mg per litre of culture *A. carboxidovorans*. This indicates that Mo-CODH is vastly more abundant in *A. carboxidovorans* (~240 times, based on purification yields), and despite this, the bacterium does not outperform *M. smegmatis* in CO oxidation rate, suggesting that Mo-CODH$_{Ms}$ is more effective at oxidising CO at low concentrations.

Next, we performed kinetic analysis of CO consumption by *M. smegmatis* and *A. carboxidovorans* cultures at low CO concentrations (2 – 600 ppm). While *M. smegmatis* cultures approached V_{max} within this concentration range, allowing us to fit the data using Michaelis-Menten kinetics, the *A. carboxidovorans* plot was linear suggesting Mo-CODH$_{Ac}$ is lower affinity (Extended Data Figure 1b,c). We then natively purified Mo-CODH$_{Ac}$ and determined its Michaelis-Menten kinetics and ability to consume CO to below atmospheric concentration (Supplementary Figure 1c,d,e). Starting at a headspace concentration of 10 ppm, Mo-CODH$_{Ac}$ was able to oxidise CO to below atmospheric concentrations (0.1 ppm), and to the limit of detection of our gas chromatograph (0.01 ppm) (Extended Data Figure 1d). Consistent with the range of previously published K_m values for Mo-CODH$_{Ac}$ (520 nM and 10.7 µM [2,3]), we calculated a K_m of 2.30 µM (95% CI 1.36 to 4.22 µM) for Mo-CODH$_{Ac}$ (Extended Data Figure 1e). This indicates that high affinity is not required for Mo-CODH to oxidise CO at atmospheric concentrations. The concentration of dissolved CO with an atmospheric (0.1 ppm) headspace is below 100 pM, meaning regardless of affinity, a Mo-CODH is acting in the

linear V vs. [S] region far below its K_m value. At this concentration, the k_{cat}/K_m ratio dominates the kinetics. These data indicate that Mo-CODHs may be generally capable of atmospheric CO oxidation. However, as observed for *M. smegmatis* and *A. carboxidovorans* cultures, higher-affinity enzymes are likely more efficient at oxidising CO at this concentration.

Supplementary Note 2. Protein film electrochemistry of Mo-CODH$_{Ms}$

Cyclic voltammograms were recorded on a Mo-CODH$_{Ms}$ film in electrolyte solutions at pH 8.0 under a N_2, CO or CO_2 atmosphere (1 bar) (Figure 1e,f). Under the N_2 atmosphere, a well-defined chemically reversible process was observed with a mid-point potential of -0.292 V (Figure 1e). In addition, two oxidation peaks were observed at the potential of -0.065 and +0.260 V, designated * and *' (Figure 1e). Under CO atmospheres, a sigmoidal-shaped catalytic oxidation process emerged at the potential region where the chemically reversible process took place (Figure 1f, red trace). These results suggest the process at -0.292 V is associated with the redox transformation of the molybdenum active centre, which involves two electrons ($Mo^{VI/IV}$)[4]. The reversible potential likely associated with the $Mo^{VI/IV}$ process is < 0.3 V more positive than the equilibrium potential of the CO_2/CO reaction (-0.580 V vs SHE at pH 8.0[5]), demonstrating the effectiveness of Mo-CODH$_{MS}$ in catalysing this process. Our electrochemical data are broadly consistent with the previous report by Bernhardt et al. on the Mo-CODH$_{Ac}$ enzyme who found the $Mo^{V/IV}$ and $Mo^{VI/V}$ processes with reversible potentials of -0.357 V and -0.165 V respectively, in an electrolyte solution containing 50 mM HEPES (pH = 7.2) based on EPR measurements undertaken at liquid N_2 temperatures[6]. We note we only resolved one peak in our PFE analysis of Mo-CODH$_{Ms}$. This could be attributable to the resolution of PFE vs EPR, or differences in redox chemistry between the enzymes. More closely spaced $Mo^{VI/V}$ and $Mo^{V/IV}$ processes than Mo-CODH$_{Ac}$ have often been found for members of the xanthine oxidase family that contains Mo-CODH, indicating the latter is a possibility [7,8]. In their study, Bernhardt et al. also found processes at more positive potential regions that were assigned to other electroactive groups, such as the FeS^{I}, FeS^{II} clusters, which may correspond to irreversible * and *' processes with oxidation peak potentials of -0.065 V and +0.260 V observed in our data. These peak potentials vary to some degree between experiments, which is not surprising for an irreversible process.

DC voltammograms of immobilized Mo-CODH$_{Ms}$ were recorded at pH 8.0 using a series of scan rates (Extended Data Figure 2a). The linearity of the peak current versus scan rate confirms that the enzyme is successfully confined on the electrode surface (Extended Data Figure 2b). To calculate the surface coverage of enzyme, we used a common baseline correction method[9]. In this method, polynomial fitting is conducted using the data available in the double-layer charging-only region of the enzyme film voltammogram to estimate the background current (Extended Data Figure 2c). For estimation of enzyme surface coverage, the faradaic current associated with the enzyme is obtained by subtracting the background from the enzyme film voltammogram (Extended Data Figure 2d). The amount of charge (Q) associated with the oxidation Mo-CODH was estimated from the peak area of the background subtracted voltammogram (Extended Data Figure 2c,d). Then, an enzyme loading (N) value of 2.2×10^{-13} moles was calculated using Faraday's law ($N = Q/(nF)$, where n and F refer to the number of electrons involved in the reaction (two in this case) and Faraday's constant, respectively.), which corresponded to a surface coverage of 2.4×10^{-12} mol/cm^2, typical for enzyme monolayers on electrodes[60].

Under a CO atmosphere, the sigmoidal-shaped steady-state voltammetric response is apparent at both 20 and 50 mV s^{-1} scan rates and the limiting current is scan rate-independent (Extended Data Figure 2e). Since these voltammograms were recorded under stationary conditions with a macro-disc electrode, this pseudo-first-order (i.e. CO concentration polarization is negligible) steady-state response suggests that the electrode process is limited by enzyme kinetics. Therefore, the steady-state limiting current (i_{ss}) can be described by the following equation:

$$i_{ss}ii_{ss} = nFN\frac{k_{cat}c}{c+K_M}kk_{cat}c\frac{k_{cat}c}{c+K_M}K\frac{k_{cat}c}{c+K_M} \qquad (1)$$

where c is the concentration of CO. Since the concentration of CO is approximately 1.0 mM at 1 bar, which is much larger than K_m, Equation 1 can be simplified as,

$$i_{ss}ii_{ss} = nFNk_{cat}kk_{cat} \qquad (2)$$

A k_{cat} of 27 s^{-1} was determined based on Equation 2. Although the activity of CODH under electrochemical conditions has been unambiguously demonstrated, we have encountered variability in the magnitude of the response between films and over time. This may be due to

the relatively rapid denaturation of enzymes when they interact with the electrode surface, which was reported previously[57]. Therefore, this k_{cat} value is indicative only and may be considered the lower limit of the true value. Given these considerations, this k_{cat} value is comparable to the value of 93.3 s^{-1} reported for the Mo-CODH from *A. carboxidovorans* (pH 7.2, 25 °C). No catalytic reduction of CO_2 was observed under CO_2-saturated conditions (see Figure 1e; blue line). This is consistent with previous work suggesting Mo-CODH is limited to CO oxidation [10,11]. The redox potential of the enzyme is much more positive than that of CO_2/CO, making the CO_2 reduction reaction thermodynamically unfavourable.

Supplementary Methods

Supplementary Method 1. Bacterial culturing: *M. smegmatis* mc^2155 WT, CoxM-strep, *ΔcoxG, ΔcoxG:pcoxG* and *ΔcoxG:pcoxG* mutant strains were grown from frozen glycerol stocks on lysogeny broth agar plates supplemented with 0.05% (w/v) Tween80 (LBT) for 3-4 days at 37°C (Supplementary Table 7). Starter cultures were inoculated with colonies from LBT plates and were grown in LBT media at 37°C and shaking at 200 rpm overnight. Broth cultures were inoculated from turbid starter cultures to OD_{600} = 0.01 and grown in Hartman's de Bont (HdB) minimal media supplemented with 0.05 % (v/v) glycerol and 0.05% (w/v) tyloxapol and incubated at 37 °C with shaking at 150 rpm. Cells were harvested at 3 days post-OD_{max} (peak Mo-$CODH_{Ms}$ expression). *A. carboxidovorans* was initially revived from glycerol stocks and grown in DSMZ 133 media supplemented with acetate. Once *A. carboxidovorans* was revived it was grown in DSMZ 133 media in a 50% CO headspace at 30 °C, shaking at 150 rpm, chemoautotrophically for seven days until the cultures reached exponential phase. 5 L of cells were grown for Mo-$CODH_{Ac}$ purification and harvested by centrifugation and stored at -20 C. 120 mL serum vials containing 30 mL of *A. carboxidovorans* in a 50% CO headspace were used for gas chromatography experiments.

Supplementary Method 2. Mutant construction: *M. smegmatis* mc^2155 chromosomal mutants were generated using allelic exchange mutagenesis as previously described [12,13]. A twin-Strep II tag was inserted at the C-terminus of the *coxM* gene (MSMEG_0744) of one strain, and a knock-out of the *coxG* gene was performed in another. 500 bp upstream and

downstream of the *coxM* C-terminus were fused to a twin-Strep II tag (5'GGCGGTTCGGGCTGGTCCCACCCCCAGTTCGAAAAGGGTGGGGGCTCCGGTGGCGGGTCGGGT GGGTCCGCCTGGTCGCACCCGCAGTTCGAGAAG 3') in a 1111 bp fragment synthesised by Genscript. Two ~500bp fragments upstream and downstream of the *coxG* gene were fused to create a deletion construct of 1011 bp and synthesised by Genscript. The fragments were cloned into the SpeI site of the mycobacterial shuttle plasmid pX33 and transformed into *M. smegmatis* mc^2155 via electroporation [12]. Transformants were grown on LBT gentamycin plates at 28°C for 7 days to allow for temperature–sensitive vector replication. Colonies from this transformation were subcultured in LBT gentamycin broth at 40°C for 3-5 days and then serially diluted from the broth onto LBT gentamycin plates and incubated at 37°C for 3–5 days. This is the first integration step which allows for the integration of the recombinant plasmid into the chromosome. Colonies were then selected and subcultured into LBT supplemented with 10% sucrose (w/v) for 3-5 days to facilitate the second recombination event. The broths were serially diluted onto LBT agar plates supplemented with 10% sucrose (w/v) and incubated at 37°C for 3–5 days. Gentamycin-sensitive colonies were subsequently screened by PCR to distinguish WT revertants from mutants. The primers used for screening are listed in Supplementary Table 7. The CoxG WT complementation plasmid was constructed by PCR of *coxG* from *M. smegmatis* mc^2155 gDNA followed by ligation into the pMV261 complementation vector using the BamHI and EcoRI restriction sites (primer sequences listed in Supplementary Table 7). CoxG complementation mutants were synthesised as gene fragments by Twist Bioscience and sub-cloned into pMV261 using the restriction sites BamHI and EcoRI.

Supplementary Method 3. PAGE analysis, activity staining and western blotting: For SDS- and native-PAGE, samples were run on Bolt 4–12% SDS-polyacrylamide and native PAGE 4-16% gels (Invitrogen) respectively, according to the manufacturer's instructions. Gels were visualized by AcquaStain Protein Gel Stain (Bulldog, AS00100), or nitrotetrazolium blue (NBT) for activity staining. For NBT activity staining, gels were in 50 mM Tris, 150 mM NaCl pH 8.0 buffer supplemented with 500 µM NBT in an anaerobic jar amended with 100% CO for 24 hours at RT. We identified Mo-$CODH_{Ms}$ activity through the purple colour of reduced NBT.

Supplementary Method 4. Mass spectrometric menaquinone detection: Purified CoxG expressed in *E. coli* was incubated with *M. smegmatis* membranes extracted from 8 L of *M. smegmatis* culture, or pure MQ9 suspended in DMSO. To prepare membranes, *M. smegmatis* mc^2155 was grown in LBT for 3 days at 37 °C and harvested by high-speed centrifugation. Pellets were resuspended in assay buffer (50 mM Tris, 150 mM NaCl pH 8.0, supplemented with plus 0.1 mg/ml lysozyme, 0.05 mg/ml DNase I, and cOmplete protease cocktail inhibitor tablets (Roche, 11836145001)) and lysed using a cell disrupter (Emulsiflex). Cell debris was pelleted by centrifugation (30,000 x g, 30 mins) and the clarified lysate was subjected to ultracentrifugation (100,000 × g, 1 hour). Membranes were resuspended in assay buffer and incubated with 5 mg of CoxG overnight at 4 °C, slowly rotating. The membranes were pelleted through ultracentrifugation again, and CoxG was repurified using Ni-affinity chromatography with a Histrap 5 mL (Cytiva, 17524801). Following loading onto the column, the resin was washed with 10× column volumes of Ni-binding buffer, and bound proteins were eluted with a step gradient of Ni-gradient buffer (50 mM Tris, 150 mM NaCl, 500 mM imidazole [pH 8.0]) of 5, 10, 25, and 50%. For MQ9 incubation, 5 mg (277 nmol) of CoxG in 50 mM Tris, 150 mM NaCl pH 8.0, was mixed with 1 mg (1,273 nmol) of MQ9 suspended in DMSO, in a final volume of 100 µL. MQ9 appeared to be sparingly soluble under these conditions and formed a waxy coating on the reaction tube. The solution was incubated overnight at 20 °C before CoxG was repurified as described for the membrane incubation. Samples corresponding to 12 µg of purified protein, together with a positive control containing MQ9 equivalent to the quantity of ligand assuming complete occupancy (calculated based on the following: m = 12 µg, MW_{CoxG} = 18 kDa, $MW_{MQ9(II-H2)}$ = 786.63 g/mol, n = 12 x 10^{-6}/18 x 10^{3} = 0.667 nmoles. As each protein contains a single ligand: n_{ligand} = 0.667 nmoles; m_{MQ9} = 0.667 x 10^{-9} x 786.63 = **524.42 ng**), were prepared for liquid chromatography-mass spectrometry (LC-MS) analysis using a modified Folch extraction. Briefly, a 50 µL solution of purified protein (~12 µg) was treated with 1000 µL of 2:1 chloroform:methanol v/v after which the mixture was shaken for 10 mins and allowed to stand for a further 50 mins. 200 µL of water was added and the mixture was shaken for 10 mins after which the sample was allowed to stand until the two phases had completely separated. The lower chloroform-rich phase was then transferred to a 2 mL sample vial and the solvent was removed under a stream of nitrogen gas. The resulting residue was reconstituted in 100 µL of 2:1 chloroform:methanol v/v and transferred to a 200 µL sample insert, the solvent was again removed and the sample reconstituted in a 7:3

mixture of LC solvent A:LC solvent B v/v. Samples were analysed using a Dionex RSLC3000 UHPLC (Thermo) coupled to a Q-Exactive Plus Orbitrap MS (Thermo) using a C18 column (Zorbax Eclipse Plus C18 Rapid Resolution HD 2.1 x 100mm 1.8 micron, Agilent, 959758-902) with a binary solvent system; solvent A = 40% isopropanol and solvent B = 98% isopropanol both containing 2 mM formic acid and 8 mM ammonium formate. Linear gradient time-%B as follows: 0 min-0%, 8 min-35%, 16 min-50%, 19 min-80%, 23 min- 100%, 28 min-100%, 30 min-0%, 32 min 0%. The flow rate was 250 µL min^{-1}, the column temperature 50°C, and the sample injection volume was 10 µL. The mass spectrometer operated at a resolution of 70,000 in polarity switching mode with the following electrospray ionization source conditions: Spray voltage 3.5kV; capillary temperature 300 °C; sheath gas 34; Aux gas 13; sweep gas 1 and probe temp 120 °C. The percentage occupancy of the ligand was estimated by comparing the peak area from the sample and the MQ9 sample.

Supplementary Method 5. Mass spectrometric identification of CoxSML: 1 µL of purified Mo-$CODH_{Ms}$ was sent to the Monash Proteomics and Metabolomics Facility for detection. Proteins were reduced with tris(2-carboxyethyl)phosphine (Pierce, PI20490), alkylated with iodoacetamide (Sigma, I1149), and digested with mass spectrometry grade trypsin (Promega, U5111). The extracted peptides were analysed by LC-MS/MS on an Ultimate 3000 RSLCnano System (Dionex) coupled to an Orbitrap Fusion Tribrid (ThermoFisher Scientific) mass spectrometer equipped with a nanospray source. The peptides were first loaded and desalted on an Acclaim PepMap trap column (0.1 mm id × 20 mm, 5 µm) and then separated on an Acclaim PepMap analytical column (75 µm id × 50 cm, 2 µm) over a 30 min linear gradient of 4–36% acetonitrile/0.1% formic acid. The Orbitrap Fusion Tribrid was operated in data-dependent acquisition mode with a fixed cycle time of 2 s. The Orbitrap full ms1 scan was set to survey a mass range of 375–1800 m/z with a resolution of 120,000 at m/z 400, an AGC target of 1×10^6, and a maximum injection time of 110 ms. Individual precursor ions were selected for HCD fragmentation (collision energy 32%) and subsequent fragment ms2 scan were acquired in the Orbitrap using a resolution of 60,000 at m/z 400, an AGC target of 5×10^5, and a maximum injection time of 118 ms. The dynamic exclusion was set at ±10 ppm for 10 s after one occurrence. Raw data were processed using Byonic (ProteinMetrics) against a protein database covering *Mycobacterium smegmatis* mc^2155. The precursor mass tolerance was set at 20 ppm, and fragment ions were detected at 0.6 Da. Oxidation (M) was set as

dynamic modification, carbamidomethyl-(c) as fixed modification. Only peptides and proteins falling below a false discovery rate of 0.01 were reported.

Supplementary Methods References

1 Bayly, K. *et al.* Mycobacteria Tolerate Carbon Monoxide by Remodeling Their Respiratory Chain. *Msystems* **6**, e01292-01220 (2021).

2 Zhang, B., Hemann, C. F. & Hille, R. Kinetic and spectroscopic studies of the molybdenum-copper CO dehydrogenase from *Oligotropha carboxidovorans*. *Journal of Biological Chemistry* **285**, 12571-12578 (2010).

3 Kaufmann, P., Duffus, B. R., Teutloff, C. & Leimkühler, S. Functional studies on oligotropha carboxidovorans molybdenum–copper CO dehydrogenase produced in *Escherichia coli*. *Biochemistry* **57**, 2889-2901 (2018).

4 Ritacca, A. G. *et al.* Unraveling the Reaction Mechanism of Mo/Cu CO Dehydrogenase Using QM/MM Calculations. *ACS Catalysis* **12**, 7336-7343 (2022). https://doi.org/10.1021/acscatal.2c01408

5 Zhang, Y., Guo, S.-X., Zhang, X., Bond, A. M. & Zhang, J. Mechanistic understanding of the electrocatalytic CO2 reduction reaction–New developments based on advanced instrumental techniques. *Nano Today* **31**, 100835 (2020).

6 Kalimuthu, P. *et al.* The oxidation-reduction and electrocatalytic properties of CO dehydrogenase from *Oligotropha carboxidovorans*. *Biochimica et Biophysica Acta (BBA) - Bioenergetics* **1861**, 148118 (2020). https://doi.org/https://doi.org/10.1016/j.bbabio.2019.148118

7 Aguey-Zinsou, K. F., Bernhardt, P. V. & Leimkühler, S. Protein Film Voltammetry of *Rhodobacter capsulatus* Xanthine Dehydrogenase. *Journal of the American Chemical Society* **125**, 15352-15358 (2003). https://doi.org/10.1021/ja037940e

8 Spence, J. T., Barber, M. J. & Siegel, L. M. Determination of the stoichiometry of electron uptake and the midpoint reduction potentials of milk xanthine oxidase at 25 degrees by microcoulometry. *Biochemistry* **21**, 1656-1661 (1982). https://doi.org/10.1021/bi00536a028

9 Jeuken, L. J. *Biophotoelectrochemistry: from bioelectrochemistry to biophotovoltaics*. Vol. 158 (Springer, 2017).

10 Fesseler, J., Jeoung, J.-H. & Dobbek, H. How the [NiFe4S4] Cluster of CO Dehydrogenase Activates CO2 and NCO−. *Angewandte Chemie International Edition* **54**, 8560-8564 (2015). https://doi.org/https://doi.org/10.1002/anie.201501778

11 Bährle, R., Böhnke, S., Englhard, J., Bachmann, J. & Perner, M. Current status of carbon monoxide dehydrogenases (CODH) and their potential for electrochemical applications. *Bioresources and Bioprocessing* **10**, 84 (2023). https://doi.org/10.1186/s40643-023-00705-9

12 Gebhard, S., Tran, S. L. & Cook, G. M. The Phn system of *Mycobacterium smegmatis*: a second high-affinity ABC-transporter for phosphate. *Microbiology* **152**, 3453-3465 (2006).

13 Grinter, R. *et al.* Structural basis for bacterial energy extraction from atmospheric hydrogen. *Nature* **615**, 541-547 (2023). https://doi.org/10.1038/s41586-023-05781-7

Supplementary Source Data Files

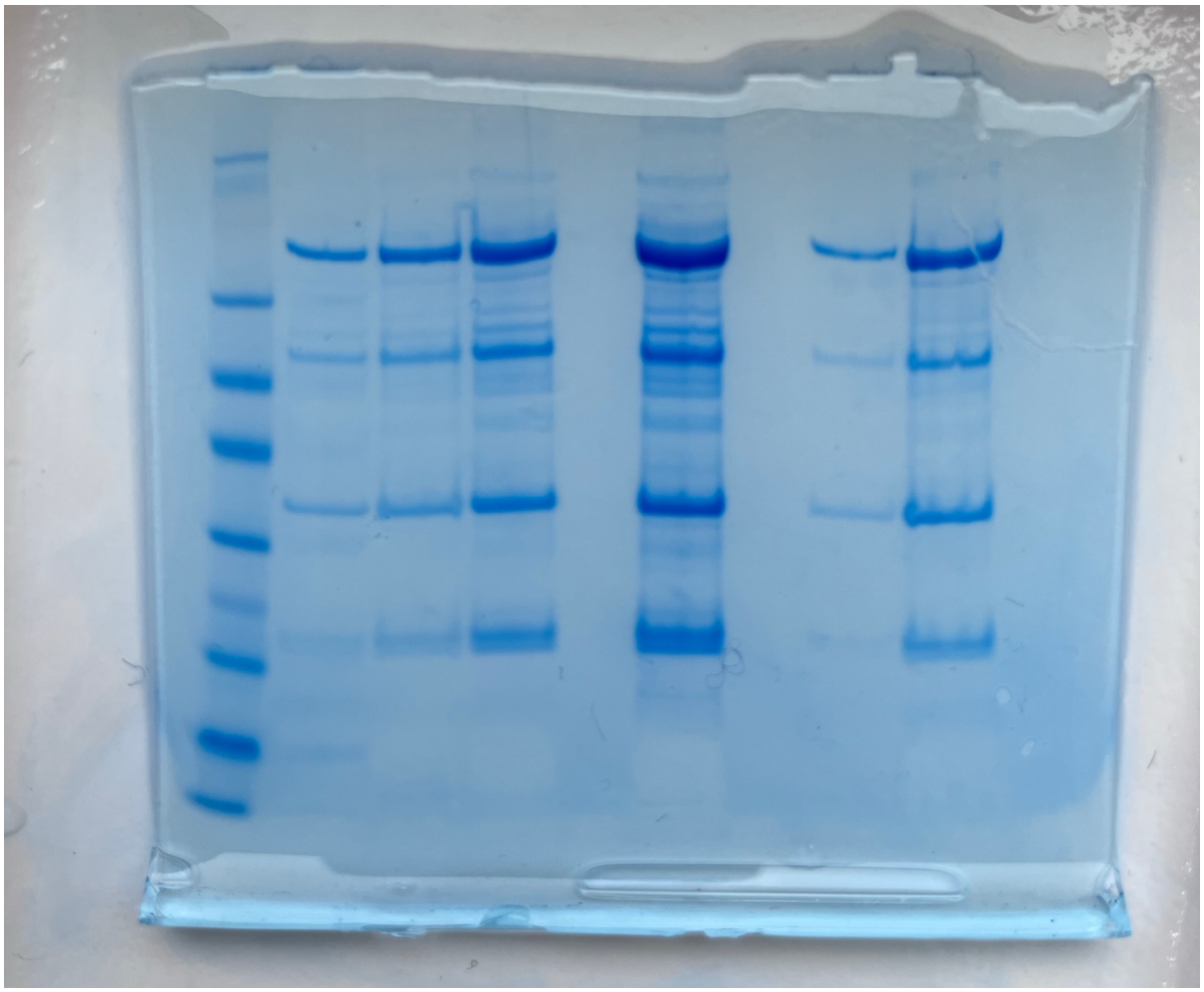

Supplementary Figure 1e.